NUCLEAR INSTRUMENTS & METHODS IN PHYSICS RESEARCH
Section A

Performance evaluation and calibration issues of large format infrared hybrid active pixel sensors used for ground and space based astronomy

Gert Finger[a*], James Garnett[b], Naidu Bezawada[c], Reinhold Dorn[a], Leander Mehrgan[a], Manfred Meyer[a], Alan Moorwood[a], Jörg Stegmeier[a], Guy Woodhouse[d]

[a]*European Southern Observatory,Karl-Schwarzschildstrasse2, D-85748 Garching, Germany.*

[b]*Rockwell Scientific, 5212 Verdugo Way, Camarillo, CA 93012, USA.*

[c]*UK Astronomy Technology Centre, Blackford Hill, Edinburgh EH9 3HJ, UK.*

[d]*CCLRC Rutherford Appleton Laboratory, Chilton, Didcot, OX11 0QX, Oxon, UK.*

Elsevier use only: Received date here; revised date here; accepted date here

Abstract

Instruments for large 10 meter class telescopes increasingly require high sensitivity large format focal planes. The high spatial resolution achieved with adaptive optics combined with multiple integral field units feeding high resolution spectrographs are driving the pixel performance and require large detector formats. In the infrared spectral range the array formats have arrived at 2Kx2K pixels with both LPE and MBE grown HgCdTe on CdZnTe substrates. In the optical, fully depleted Si-PIN diodes of the same format are used. The light sensitive diode arrays are hybridized to CMOS FET switched multiplexers such as the Hawaii-2RG array, which has recently been installed in one of the infrared instruments of the Very Large telescope VLT. Basic performance characteristics of the Hawaii-2RG arrays will be discussed such as the noise performance when a special technique of using reference pixels is employed. Larger focal planes are realized as mosaics of 2Kx2K arrays. In order to increase the format of single arrays to 4Kx4K and larger, the limited substrate sizes makes it necessary to reduce the pixel size. However, with smaller pixels the coupling between pixels becomes a limiting factor for the detector point spread function. Fundamental calibration issues relevant to photon transfer techniques of modern CMOS active pixel sensors with special regard to the influence of inter-pixel coupling capacitances will be analyzed in detail. A novel technique will be presented to directly measure the point spread function generated by the capacitive coupling between adjacent pixels.

[*]Corresponding author. Tel.: +49-89-32006256; fax: +49-89-32006530; e-mail: gfinger@eso.org.

Keywords: conversion gain; interpixel capacitance; Hawaii-2RG; HgCdTe; point spread function; quantum efficiency; raedout noise;

1. Introduction

An infrared hybrid active pixel sensor is composed of two components, a diode array fabricated with narrow band gap semiconductor material sensitive at infrared wavelengths and a silicon CMOS readout multiplexer with a buffer source follower, a reset switch and addressing switches placed in the unit cell of each pixel. The two components, the infrared diode array and the Si CMOS multiplexer are hybridized with In bumps making the electrical interconnections for each pixel between the infrared diode and the unit cell of the Si multiplexer [1].

Currently three semiconductor materials achieve the highest performance for detectors used in infrared astronomy For most scientific applications the wavelength range below 1μm is still dominated by silicon CCD's, yet the performance of silicon PIN diode arrays hybridized to Si readout multiplexers is rapidly improving and has some advantages with respect to versatility, quantum efficiency at the cutoff wavelength and readout speed. In the near infrared spectral range from 1 to 5 μm, two semiconductor materials are competing, namely InSb and HgCdTe grown by liquid phase epitaxy (LPE) or molecular beam epitaxy (MBE) on Al_2O_3, Si or CdZnTe substrates. Extrinsic blocked impurity band Si:As arrays cover the mid infrared spectral range from 8 to 28 μm [1]. This paper will focus on HgCdTe arrays grown on CdZnTe substrates.

The European Southern Observatory ESO has established a long lasting collaboration with the two main manufacturers of scientific infrared sensors, namely Rockwell Scientific and Raytheon Vision Systems. ESO is well equipped for assessing all aspects of the sensor performance relevant to ground and space based astronomy. The results of the detector evaluation is taken into account by the manufacturers to improve and optimize the arrays for astronomical applications.

In order to achieve the highest sensitivity with infrared instruments, the detector dark current must be negligible in comparison to the photon generated current (< 10 e/hour). The readout noise should be small in comparison to the photon shot noise (< 3 e rms). The interpixel crosstalk and the effect of latent image effect should be as small as possible, whereas the quantum efficiency should be close to 100%. Recent inconsistencies [2] encountered with modern CMOS arrays having pixels as small as 18 microns triggered a more thorough investigation of the applicability of standard calibration methods which will be described in chapter 4 below.

2. Limitations of array format

The high spatial resolution provided by adaptive optics on large telescopes having diameters in the range of 10 to 100 m requires extremely large focal planes of up to more than 10^9 pixels in order to Nyquist sample [3] diffraction limited images. At present the focal plane technology has arrived at formats of 2Kx2K.

Two major problems are to be solved when the format of hybrid active pixel sensors is increased. Firstly, the mating force that has to be applied to the hybrid components to produce a robust indium interconnect bond scales with the detector format. Secondly, when hybrids employing intrinsic narrow bandgap materials are cooled to cryogenic temperatures, they have to withstand the thermal mismatch between the infrared active material, the detector substrate and the Si readout multiplexer, all of which have different coefficients of thermal expansion (CTE).

The size of available detector substrates will eventually impose a limit on the format of detectors. Presently, CdZnTe substrates with 60 mm diameter limit the format of HgCdTe arrays to 2Kx2K. Alternative substrates for HgCdTe such as Si and Al_2O_3 constitute a viable approach to larger formats, but limit the pixel performance because of higher dislocation densities due to the imperfect lattice match of the detector material and the substrate.

Hence, the detector manufacturers tend to shrink the pixel size from 20 μm to 10 μm to accommodate larger array formats on the limited space of the biggest detector substrates. The advances in In bump

technology permit pixel sizes of 10 μm. However, if the pixel size is shrinking, other effects limiting the detector performance such as the interpixel capacitance are becoming more important. The effect will be discussed in some detail in section 4.

An alternative to increasing the number of pixels in focal planes is the installation of closely packed mosaics. An example for an array mosaic currently under development is the VISTA focal plane, which is being built for the Infra-Red Survey Telescope VISTA by the UKATC and RAL for ESO [4][5].

VISTA is a wide field survey telescope which has a diameter of 4 meters. It will initially be dedicated to IR imaging surveys. The focal plane is located in the Cassegrain focus and is populated with 16 2Kx2K science detectors packed at 90% spacing in one direction and 42.5% in the other. The VIRGO detector produced by Raytheon has been selected for VISTA. It is a LPE HgCdTe array grown on a CdZnTe substrate. The CdZnTe substrate provides an excellent lattice match for the IR active HgCdTe layer resulting in low defect densities and stacking faults. The pixel size is 20 μm. Each detector has 16 parallel outputs organized in parallel stripes, which can be read at a pixel rate of 400 KHz. The total channel count adds up to 256 channels. The scaleable ESO controller IRACE is used to read out the complete VISTA focal plane at a frame rate of up to 1.6 Hz. All 16 science grade arrays have been delivered and tested at UKATC. The quantum efficiency of the best arrays is 85% at 1.2 μm and above 95% between 1.75 and 2.5 μm. The detector dark current is 0.03 e/s/pixel at an operating temperature of 77 K. Figure 1 shows the VISTA focal plane at Rutherford Appleton Laboratory which is partially populated with 4 bare Si multiplexers having no IR active layers and two hybridized engineering grade 2Kx2K HgCdTe VIRGO arrays [6]. The aluminum plate shown in Figure 1 has since been replaced by the real molybdenum plate.

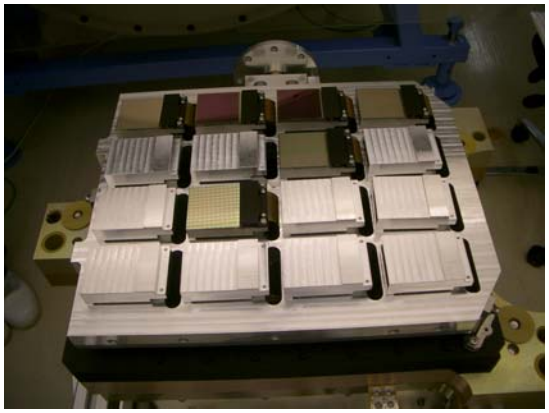

Figure 1 VISTA mosaic of 16 2Kx2K arrays populated with 4 bare Si multiplexers having no IR active layers and two hybridized engineering grade 2Kx2K HgCdTe VIRGO arrays.

3. Performance of the Hawaii-2RG array

The Hawaii-2RG array is a 2Kx2K HgCdTe array produced by Rockwell Scientific and has been developed for the 6.5m James Webb Space Telescope JWST, the successor of the Hubble space telescope. It will operate in the λ=1 – 2.5 μm and 1 – 5 μm spectral range [7].

The Hawaii-2RG array combines the most advanced silicon multiplexer with a new growth technology for infrared diode arrays. Instead of using liquid phase epitaxy the Hawaii-2RG arrays are grown by molecular beam epitaxy on CdZnTe substrates. The infrared arrays are double layer planar heterostructures with a wide bandgap capping layer. In comparison to LPE material grown on Sapphire (PACE material) the new growth technology has lower defect densities. As a consequence, the detector dark current is reduced substantially. The arrays have high quantum efficiency over their entire sensitive spectral range. The MBE growth process on a lattice matched CdZnTe substrate was also expected to reduce the persistence effect. Unfortunately, this expectation is not fully met for λ_c=2.5 μm arrays.

The first Hawaii-2RG array is already generating scientific results in one of ESO's instruments at the Very Large Telescope VLT, the integral field spectrograph SINFONI [8]. Three more instruments, the wide field imager Hawk-I which will house a 2x2 mosaic [9], the multi-integral field spectrograph KMOS [10], and the infrared arm of the X-Shooter spectrometer, which observes all wavelengths from UV to K-band simultaneously, will all be equipped with λ_c=2.5 μm HgCdTe Hawaii-2RG arrays [11].

3.1. Setup for the Hawaii-2RG array

A 34-channel detector package was developed for the Hawaii-2RG multiplexer interfacing all 32 video channels plus one extra channel for the guide mode and one for the reference pixel. Since the SIDECAR ASIC developed by Rockwell for the Hawaii-2RG detectors was not yet available [12] for ESO, in our set-up we placed symmetric cryogenic CMOS operational amplifiers next to the focal plane and accessed the internal bus of the detector directly, bypassing the on-chip buffer amplifier [13].

For the wide field camera Hawk-I the focal plane will be equipped with a 2x2 mosaic of Hawaii-2RG arrays. A modified GL Scientific mosaic module originally developed for JWST is used (see Figure 2). Four miniaturized PCB detector boards with the 34-channel preamplifier for each detector will be placed below the mosaic in preamplifier boxes operating at cryogenic temperatures in separate light tight housings.

For JWST a dedicated ASIC, the SIDECAR chip will be used. It packs a complete detector controller including freely programmable clock and bias generation as well as 16 bit analog to digital conversion of all 34 outputs of the Hawaii-2RG on a single ASIC chip [14]. The user communicates with the ASIC through an LVDS or CMOS digital interface. Apart from simplifying the detector system the biggest advantage of the ASIC is the fact that the high impedance low level video signals are digitized directly on the focal plane and do not have to be transmitted over long cables to the ADC's of an external controller. Thus, avoiding EMI and noise pick-up, a robust system achieving excellent noise performance is expected. The first ASIC's will become available at the end of 2005.

Figure 2 Mosaic of 2x2 2Kx2K Hawaii-2RG HgCdTe arrays.

3.2. Dark current

A two stage pulse tube was used to cool the Hawaii-2RG HgCdTe array. To carry out the dark current measurements the detector was completely enclosed in a black anodized aluminum box. As can be seen in Figure 3, the dark current is < 0.01 e/sec at temperatures below 80 K (filled triangles). For comparison the dark current measured with a λ_c=2.5 µm Hawaii-2 LPE/Al_2O_3 science grade array (filled squares in Figure 3), a Hawaii-1 LPE/Al_2O_3 science grade array (empty squares in Figure 3), and a λ_c=1.7 µm PICNIC MBE/CdZnTe array (triangles) are also shown. Note the dark current of the PICNIC array was scaled to a pixel size of 18 µm. At an operating temperature of 100K, the dark current of MBE/CdZnTe arrays with λ_c=2.5 µm is a factor of 1660 times lower than that of LPE/Al_2O_3 arrays. This improvement is of particular importance for instruments which do not have closed cycle coolers but have to manage with liquid nitrogen bath

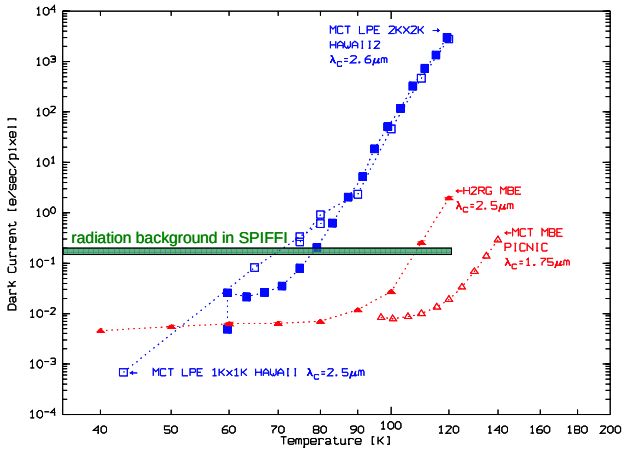

Figure 3 Dark of HgCdTe arrays current versus temperature. Squares: LPE material. (empty squares is Hawaii1 1Xx1K and filled squares is Hawaii2 2Kx2K). Triangles: MBE on CdZnTe substrate. (filled triangles is λ_c=2.5 µm Hawaii-2RG array and empty triangles is λ_c=1.7 µm PICNIC array).

cryostats. Even for low flux spectroscopic applications science grade arrays of good cosmetic quality can be operated at a temperature of 80 K.

3.3. Readout noise

The readout noise for simple double correlated sampling is 17 electrons rms for infrared active pixels. The infrared active pixels of the Hawaii-2RG array are surrounded by 4 rows and columns of reference pixels at the edges of the array. The signal of these pixels is embedded in the regular video signal of 2048 x 2048 pixels. Therefore, the active area consists of 2040 x 2040 light sensitive pixels. The reference pixels can be used to track low frequency noise pick-up. Unlike standard infrared-active pixels, the reference pixels are not connected to detector photodiodes. Instead, they contain a simple capacitor C_{pix} whose capacitance is similar to the detector capacitance. The readout noise measured on these reference pixels at the edges of the array is only 8 electrons rms. This proves that the contribution of the readout multiplexer and the rest of the data acquisition chain including the preamplifiers and the IRACE electronics to the overall readout noise is small. The readout noise is dominated by the noise of the infrared pixel. Figure 4 shows a noise map at the edge of the array. The darker left four columns at the left edge of the array are reference pixels.

Since all 32 video channels are used and the Hawaii-2RG array is organized in 32 stripes of 2048 rows, the rows of a single stripe contain only 64 pixels. If the array is read out at a frame rate of 1.2 Hz the reference pixels are read every 400 μs, which is the time needed to read a single row. Four embedded reference pixels read at the beginning and four reference pixels read at the end of each row are averaged and routinely subtracted from the video signal for all readout modes. Depending on the spectral distribution of low frequency pickup this improves the readout noise by up to a factor of two.

Multiple sampling techniques substantially reduce the readout noise as can be seen in Figure 5 which shows the readout noise versus the number of nondestructive readouts. Active infrared pixels are represented by squares; the reference pixels by triangles. The readout time for a single non-destructive readout is 825 ms. The detector is continuously read out in the nondestructive mode. The detector integration time for 1024 Fowler pairs is 845 seconds. The lowest readout noise on the active infrared pixels is 2.3 e rms with 256 Fowler pairs, whilst it is 1.3 e rms for reference pixels. Both noise values are referenced to the nodal capacitance C_0 (refer to section 4).

This outstanding noise performance impressively demonstrates two accomplishments of the Hawaii-2RG multiplexer design. First, the shielding of the multiplexer glow, which because of glow-induced photon shot noise had limited the number of Fowler pairs to < 32 with previous multiplexers, has been implemented very effectively in the Hawaii-2RG device. Second, the implementation of 32 parallel video channels not only reduces the readout time, but also improves the noise performance, since more non-destructive readouts can be made within a given integration time. This results in a further reduction of the readout noise.

The shielding of the multiplexer glow is not perfect. For larger numbers of nondestructive readouts a few localized glow centers appear at random locations across the array. The glow centers have a ring-like structure. The intensity of the glow centers linearly depends on the number of

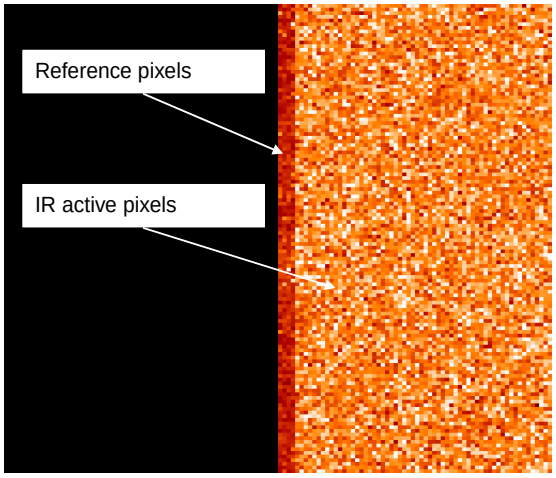

Figure 4 Noise map with reference pixels at the left edge. Readout noise on active pixels: 17 erms. Readout noise on reference pixels at left edge: 8 erms.

nondestructive readouts. Good science grade arrays are devoid of these glow centers. The absence of glow centers is an important selection criterion for science grade arrays.

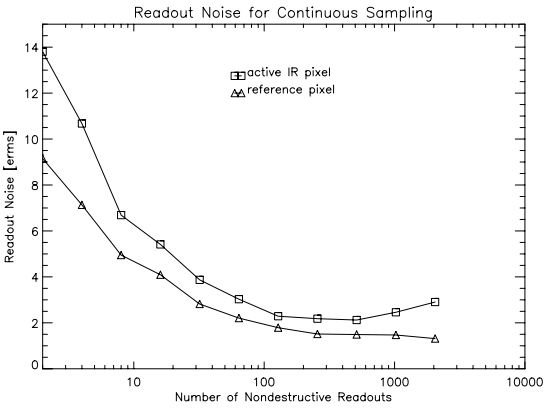

Figure 5 Readout noise versus number of nondestructive readouts. Squares are the active infrared pixels. Triangles are the reference pixels. Readout time for single readout is 825 ms. Lowest readout noise on active IR pixel is 2.3 e rms with 256 Fowler pairs. Lowest readout noise on reference pixels is 1.3 e rms.

3.4. Quantum Efficiency

The quantum efficiency is determined by illuminating the detector with a defined number of photons N_{phot} at a specific wavelength and measuring the number of photon generated electrons N_e. As shown by equation Eq. (1) the number of electrons can be retrieved from the signal voltage V_{signal} , if the conversion gain C_0/e is known, where C_0 is the nodal capacitance on which the charge is integrated, and e the charge of the electron.

$$QE = \frac{N_e}{N_{phot}} = \frac{\frac{C_0}{e} V_{signal}}{N_{phot}} \quad (EQ\,1)$$

The calibrated photon flux is generated by a blackbody of known temperature. The blackbody illuminates a grating monochromator. The wavelength dependence of the efficiency of the monochromator is monitored by a spectrally flat pyroelectric detector.

The quantum efficiency (QE) of MBE material does not depend on temperature whereas the QE of LPE material drops when cooled from 80K to 40K.

Hence, the cosmetic quality of MBE engineering grade arrays can be enhanced without loss of quantum efficiency by reducing the operating temperature. Figure 6 shows the QE as function of wavelength measured with broad band filters and with a monochromator. The conversion gain was determined with the capacitance comparison method discussed in section 4.2 since the standard shot noise method is incorrect and yields quantum efficiencies larger than 100%. For the science grade detector the quantum efficiency is 84% in K, 78% in H, 71% in J and 80% in Z. The Hawaii-2RG arrays outperform CCD's in Z band.

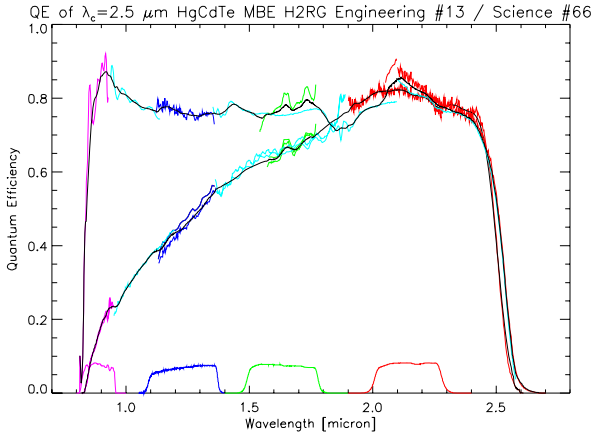

Figure 6 Quantum efficiency of λc=2.5 μm Hawaii-2RG engineering grade and science grade arrays. Transmission of band-pass filters is indicated at the bottom.

4. Calibration issues of CMOS hybrid sensors

4.1. Conversion gain by shot noise

A basic parameter characterizing the performance of CMOS hybrid active pixel sensors is the conversion gain C_0/e measured in units of electrons

per Volt. C_0 is the nodal capacitance of the integrating node of the detector pixel. All other parameters such as readout noise, dark current and quantum efficiency depend on the accurate determination of the conversion gain. Since the measurement of the quantum efficiency of CMOS hybrid arrays often leads to inconsistent results with quantum efficiencies exceeding 100% [15], we tried to narrow down the errors of all factors influencing the quantum efficiency such as the radiation geometry, the blackbody calibration, the temperature dependence of the filter transmission, radiation leaks of filters, etc. However, it was not possible to obtain a quantum efficiency in K-band of a λ_c=2.5µm HgCdTe Hawaii-2RG array below 105%.

The remaining major uncertainty is the conversion gain C_0/e. The nodal capacitance C_0 is composed of the voltage dependent diode capacitance of the detector pixel and the fixed gate capacitance of the unit cell source follower gate. It is usually determined by the widely used shot noise method assuming photon shot noise limited performance of the detector. Photons are governed by Poisson statistics with the variance of the integrated number of photons equal to the mean number of photons. For this case, the nodal capacitance C_0 can be calculated from the slope of the plot of noise squared signal versus mean signal according to Eq. (2). However, this equation only holds true if the signals of neighboring pixels are uncorrelated as explained in section 4.4.

$$C_0 = e\frac{\langle V \rangle}{\langle V^2 \rangle} \qquad (EQ\ 2)$$

4.2. Conversion gain by capacitance comparison

In order to obtain the nodal capacitance C_0 by a direct measurement which does not rely on statistical methods, a simple technique has been developed; it is based on comparing the voltage change of a large calibrated external capacitor to that of the unknown nodal capacitance C_0 which is many orders of magnitude smaller.

During normal operation the reset voltage V_{reset} is connected to an external bias voltage of the detector control electronics and the bias provides the charge required to reset the integrating node capacitor. The hardware setup for the capacitance comparison simply entails adding a switch (relay) between the bias and V_{reset} and adding a calibrated capacitor between V_{reset} and detector substrate voltage D_{sub} as shown in Figure 7. The external capacitor is then charged to the nominal reset voltage and disconnected (using the relay) from the external bias. The charge to reset the nodal capacitor C_0 of each pixel slowly discharges the external capacitor, C_{ext}.

$$\Delta V_{ext} C_{ext} = \sum_{n=1}^{n_{frames}} \sum_{i=1}^{2048} \sum_{j=1}^{2048} V_{n,i,j} C_0 \qquad (EQ\ 3)$$

If the 2Kx2K pixels of the detector are exposed to a high photon flux and several frames are read out and reset, the charge to repeatedly reset the complete array will discharge C_{ext} sufficiently to generate a voltage drop ΔV_{ext} across C_{ext} large enough to be accurately measured [12].

Since the voltage drop ΔV_{ext} on C_{ext} and the signals of each pixel $V_{i,j}$ are known, the nodal capacitance C_0 and thus the conversion gain C_0/e can be calculated as shown in Eq. (3). The ratio of nodal capacitance C_0 and the external capacitance C_{ext} is

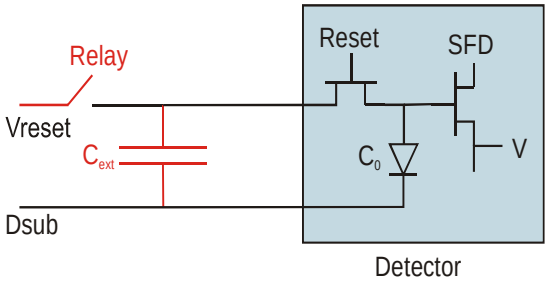

Figure 7 Hardware setup of capacitance comparison method for the measurement of the conversion gain

equal to the ratio of the voltage drop across the external capacitance ΔV_{ext} and the total integrated detector signal.

A capacitance of 9.26 µF was used for C_{ext}. It is much larger than the sum of the capacitance of all cables and other stray capacitances. The capacitances of these components may therefore be neglected.

The discrepancy of nodal capacitances C_0 determined by the capacitance comparison and the shot noise method is substantial (> 20% for HgCdTe and more than a factor of two for Si-PIN arrays) as can be seen in Table 1.

Table 1 Comparison of conversion gains C_0/e and nodal capacitances C_0 of CMOS hybrid arrays determined by capacitance comparison and shot noise method

Method:	Capacitance comparison		Shot noise	
diode array	C_0 / e [e/mV]	C_0 [fF]	C_0 / e [e/mV]	C_0 [fF]
λ_c=2.5µm HgCdTe	201 +/- 8	33.5	255.3 +/- 10	40.9
Si-PIN HyViSI	86.8 +/- 3.5	13.9	177.9 +/- 7	28.5

Nodal capacitances obtained with the capacitance comparison method (Table 1) yield a quantum efficiency for the HgCdTe Hawaii-2RG array in K-band of 86% instead of 105%, the value derived with the shot noise method. The shot noise method does not yield plausible quantum efficiency using conversion gains derived from the standard "noise squared versus signal" technique.

4.3. Conversion gain by Fe55

In an effort to compare and validate the two methods of deriving the conversion gain we used the K_α line of Fe^{55} which generates a well known number of electrons per absorbed x-ray photon and has been in use for many years to calibrate the conversion gain of optical CCD's [16]. Unfortunately, the Fe^{55} method cannot be applied to the HgCdTe arrays because the CdZnTe substrate absorbs the x-rays of the Fe^{55} source before they reach the depletion region of the infrared diodes. For the Si-PIN diode array, however, the Fe^{55} calibration is applicable. A histogram showing the number of electrons generated by the absorption of one X-ray photon is shown in Figure 8. The solid curve represents the histogram generated using the nodal capacitance C_0 determined by the capacitance comparison method; the dashed curve shows the histogram of the same data set but using the nodal capacitance determined by the standard photon transfer curve (shot noise) technique. The accepted value used in calibrating CCD's is shown as a vertical line in Figure 8. It is evident that the capacitance comparison method is consistent with the Fe^{55} value cited in the literature. The shot noise method using "noise squared versus signal" can only be applied if the coupling between pixels due to the interpixel capacitance can be neglected as explained in the next section.

The Fe^{55} method can also be applied to InSb detectors which do not have a detector substrate. First measurements yield a value of 2500 electrons per absorbed K_α x-ray photon. Possibly, the Fe^{55} method will also be applicable to HgCdTe arrays, if their substrate is removed. Further development in this area is needed.

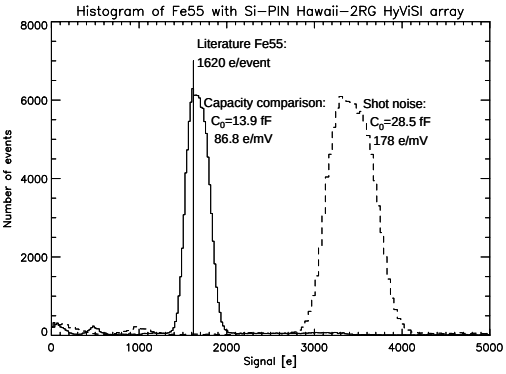

Figure 8 Histogram of Hawaii-2RG Si-PIN HyViSI array exposed to Fe55 X-ray source. The same data set is plotted with nodal capacitances derived from capacitance comparison method (solid histogram) and the shot noise method (dashed histogram). Literature value is indicated as a vertical line.

4.4. Conversion gain and interpixel capacitance

The nodal capacitance C_0 derived with the shot noise method appears to be too large. Since Eq. (2) shows that C_0 is inversely proportional to the variance, the measured variance of the detector signal $\langle V^2 \rangle$ should be larger to obtain a smaller but more plausible nodal capacitance, i.e., the shot noise method appears to have too low a signal variance. The discrepancy cannot be explained by excess noise of the data acquisition chain as more noise would

only make the variance larger not smaller. On the contrary, a mechanism has to be introduced which does not change the signal charge but reduces the photon shot noise of a single pixel. The larger capacitance seen by the shot noise may be explained by coupling capacitance between neighboring pixels. As a consequence of the interpixel capacitances the signal of the pixel which is hit by a photon is spread by capacitive coupling to adjacent pixels, which reduce the apparent photon shot noise. While the mean signal remains unchanged the variations about the mean are "smoothed" by the capacitive coupling to neighboring pixels. Hence, the photon shot noise method does not yield the pixel capacitance C_0, but the sum of C_0 and all the coupling capacitors in series with the nodal capacitors of the neighboring pixels as shown in Figure 9.

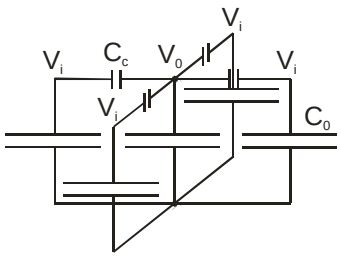

Figure 9 . Interpixel coupling capacitance. Only next neighbors are considered.

Using the coupling capacitance C_c and the ratio of coupling capacitance and nodal capacitance $x = C_c/C_0$, a simple model of the apparent capacitance C seen by the shot noise is $C = C_0(5x+1)/(x+1)$. For simplicity, only coupling to the 4 closest neighbors is considered here. By applying Kirchhoff's laws it can also be shown, that the total signal with coupling V_0+4V_i is equal to the total signal V without coupling, i.e., $V_0+4V_i = V$ with V the signal for $C_c=0$. This implies that the interpixel capacitive coupling conserves photometry. For uniform illumination of the array no signal charge is stored on the coupling capacitors. The coupling capacitors reduce the photon shot noise because the voltage response of a photon-generated electron is not confined to a single pixel, but spread over all neighboring pixels. This nominal reduction of noise is accompanied by reduced image contrast and degraded detector MTF.

4.5. Conversion gain by autocorrelation

A. Moore et al. have examined the detector edge spread and MTF; they were the first to introduce interpixel coupling as one mechanism to degrade the point spread function of CMOS detectors [17]. They devised a stochastic method of measuring the interpixel coupling using 2D autocorrelation and arrived at the same conclusion regarding the overestimation of the nodal capacitance by the shot noise method. We have applied their autocorrelation method to both HgCdTe and Si-PIN diode arrays hybridized to the Hawaii-2RG multiplexer. The autocorrelation function for both arrays is shown in Figure 10. If the difference of two uniformly illuminated shot noise limited images have pixel intensities $V_{i,j}$, and $R_{m,n}$ is the autocorrelation function, the factor φ by which the nodal capacitance is overestimated by the shot noise method using "noise squared versus signal", is given in Eq. (4)

$$\varphi = \sum_{m,n} R_{m,n}$$

$$R_{m,n} = \frac{\sum_{i,j} V_{i,j} V_{i+m,j+n}}{\sum_{i,j} V^2{}_{i,j}} \quad (EQ\ 4)$$

If the signals of neighboring pixels are not correlated, all the cross products $V_{i,j}V_{i+m,j+n}$ with $m \neq 0$ and $n \neq 0$ are 0. Hence, the interpixel capacitance is negligible. For this case φ is 1 and the "noise squared versus signal" method yields the correct nodal capacitance. If, however, there is a correlation between neighboring pixels due to coupling capacitances, the correct nodal capacitance can still be derived from the shot noise of difference images by properly taking the correlation between pixels into account, which is expressed by the correction factor φ given in Eq. (4).

We determined the correction factors φ for the nodal capacitance of CMOS hybrids with the 2D

autocorrelation method of A. Moore. The measured values are φ_{HgCdTe}=1.20 for the HgCdTe array and $\varphi_{Si\text{-}PIN}$=2.03 for the HyViSI Si-PIN array. Both arrays are hybridized to the same type of Hawaii-2RG multiplexers. The correction factors are in good agreement with the results given in table 1 and further support the results obtained with the capacitance comparison method.

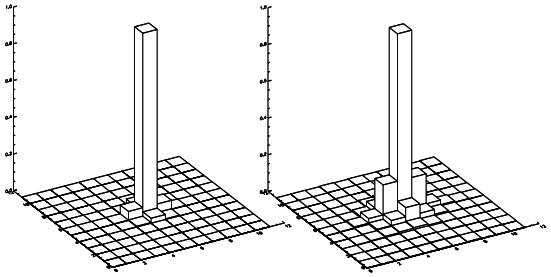

Figure 10. Autocorrelation of CMOS Hawaii-2RG hybrid arrays. Left: λ_c=2.5 µm HgCdTe array, φ = 1.23 +/- 0.06. Right: Si-PIN HyViSI array, φ = 2.03 +/-0.1.

4.6. Point spread function of interpixel capacitance

The Hawaii-2RG multiplexer has a unique feature, the guide mode, which is implemented for telescope guiding and correction of fast image motion induced by atmospheric turbulence. The guide mode operation allows simultaneous operation of the full array read out at a frame rate of 1 Hz and a small sub-window read out at frame rates of a few hundred Hz. Since the reset of the small guide window can be controlled independently from the full frame, this feature makes it possible to determine in a very direct way the point spread function (PSF) generated by capacitive coupling between adjacent pixels [18].

If the size of the guide window is reduced to a single pixel which is reset at a much higher frequency than the full 2Kx2K array, which is uniformly illuminated, the integration time for the guide window pixel is much shorter than for the full array. Consequently, the signal of the guide window pixel will be almost zero, whereas all other pixels will have integrated a large number of photon generated charge. Using the annotation of Figure 9 and assuming the guide window pixel is the central pixel, the voltage V_0 of the guide window pixel will be almost zero and the voltage for all other pixels will be large and uniform, except for the pixels very close to the guide window pixel. Depending on the ratio of the coupling capacitance C_c and the nodal capacitance C_0, the capacitive voltage division will slightly reduce the signal of the neighbors surrounding the guide window pixel. The normalized difference of two images, one taken with the reset of the guide window pixel switched on and one taken without resetting the guide window pixel, directly yields the point spread function generated by the capacitive coupling of the interpixel capacitance. In Figures 11 and 12 the PSF obtained in this way is shown for two arrays, both of them hybridized to the same Hawaii-2RG multiplexer, on the left side the PSF of a HgCdTe array and on the right side the PSF of a Si-PIN diode array. Figure 11 shows the photometry and Figure 12 a surface plot of the normalized PSF. The interpixel coupling of the HgCdTe array spills 2.5% of the single pixel signal to the next neighbors and the total signal integrated over all pixels is 1.10, which means, that 10% of the signal of each pixel is spread over the neighboring pixels.

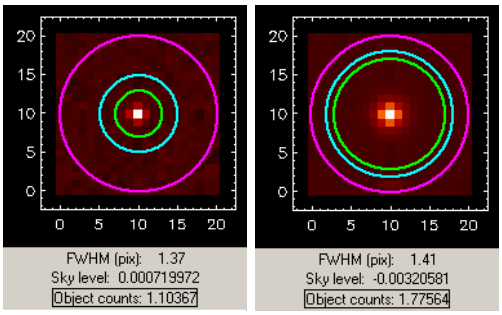

Figure 11 Photometry of normalized point spread function of interpixel capacitance by single pixel reset using the guide window mode. Left: 2Kx2K Hawaii-2RG HgCdTe array. Total signal 1.10 Right: 2Kx2K Hawaii-2RG Si-PIN array HyViSI. Total signal 1.78. Signal of central pixel is 1.

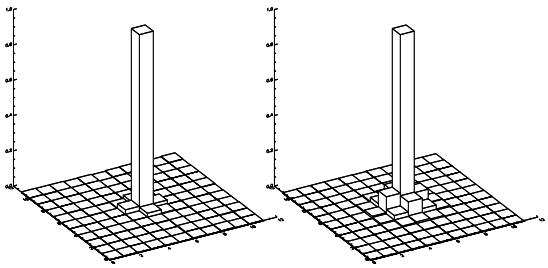

Figure 12 Normalized point spread function of interpixel capacitance measured by single pixel reset using the guide window mode. Left: 2Kx2K Hawaii-2RG HgCdTe array. Right: 2Kx2K Hawaii-2RG Si-PIN array HyViSI.

The interpixel coupling of the Si-PIN diode arrays shown on the right side of Figures 11 and 12 is 8 times larger than the corresponding value for infrared arrays. The total signal integrated over all pixels is 1.78 which means that 78% of the signal of each pixel is spread over its neighbors. Each of the 4 closest neighbors above and below the guide window pixel receives 10% and the pixels in the corners still get 3%. At a distance of two pixels capacitive coupling is 1%.

In HgCdTe arrays each pixel diode maintains its own local depletion region. Adjacent pixels are separated by the n-doped bulk of HgCdTe which is conducting. Since no electric field can build up between pixels, they are screened from each other. Capacitive coupling can only occur in the space between the infrared array and the Si multiplexer between the In-bumps and to some extent also within the multiplexer itself.

In the Si-PIN diode array of the HyViSI detector the bulk of the silicon is fully depleted and the electric fields can also build up between pixels resulting in the large observed interpixel capacitance. Since the Si-PIN HyViSI array uses similar In bumps and exactly the same multiplexer as the HgCdTe array, but exhibits much stronger interpixel coupling, it may be assumed that the main coupling occurs inside the Si-PIN diode array.

The single pixel reset measurement is also sensitive to the readout speed. Enough settling time has to be given to the video signal. In our experiment the detector was operated at a frame rate of 0.59Hz and multiple sampling was used to improve the signal to noise ratio.

It is planned to measure the PSF with the single pixel reset as a function of reverse bias voltage for both HgCdTe and Si-PIN diode arrays to investigate the effect of the electric field on the interpixel capacitance. To complement the measurement of the PSF obtained with the single pixel reset the optical PSF, which is composed of all contributions, the capacitive coupling between pixels as well as charge diffusion and optical crosstalk, has to be measured as well.

5. Conclusions

The demand for extremely large focal planes on modern telescopes has driven the array format to 2Kx2K, a limit which cannot be surpassed easily because of limited substrate sizes. Therefore, larger focal planes are usually built up as mosaics. Modern 2Kx2K HgCdTe arrays grown by LPE or MBE on CdZnTe substrates have high QE (>80%) and extremely low dark currents (< 0.01 e/s/pixel at T=80K) but are still suffering from latent images if previously exposed to bright light sources. The readout noise of the Hawaii-2RG MBE arrays is 17 e rms for double correlated sampling. However, the shielding of the multiplexer glow is very effective and allows multiple sampling techniques using 256 Fowler pairs. This reduces the readout noise to 2.3 e rms.

Since the size of available substrates is limited, the only way to increase the format of modern CMOS hybrid arrays to 4Kx4K and beyond is to revert to smaller pixels in the range of 10 – 15 μm. This leads to other limitations such as the coupling capacitances between neighboring pixels which become more important for smaller pixels. Even if the interpixel capacitance is only a few percent of the nodal capacitance of a detector pixel, the coupling capacitance has to be taken into account to obtain the correct conversion gain with stochastic methods. The usual “noise squared versus signal” method leads to an overestimation of the nodal capacitance of 20% for infrared arrays and 100% for Si-PIN diode arrays. An alternative method of measuring the nodal capacitance, the capacitance comparison technique, is the most direct method and is also simple to implement. It delivers nodal capacitances which yield plausible quantum efficiencies below 100% for both HgCdTe and Si-PIN hybrids. Furthermore, the method is consistent with the 1620 electrons generated in silicon PIN diodes by the absorption of K_α x-ray photons emitted by Fe^{55}. Additional confirmation for the capacitance comparison method comes from a stochastic method based on 2D autocorrelation to determine the nodal capacitance.

The guide mode of the Hawaii-2RG array makes it possible to apply a single pixel reset and directly measure the point spread function generated by capacitive coupling between adjacent pixels. With

this technique a coupling capacitance smaller than 1fF can be easily measured. Contrary to optical crosstalk and charge diffusion, which also contribute to interpixel crosstalk, capacitive coupling between detector pixels is a deterministic process. Hence, the PSF caused by this effect, which can be measured with the single pixel reset method on Hawaii-2RG arrays, can directly be used to deconvolve images.

In the photon noise limited regime both the signal and the noise are attenuated by the same factor due to interpixel capacitance. However, for point sources in the read noise limited regime the spreading of the signal response to neighboring pixels seriously affects the signal to noise ratio and degrades the detector MTF and image sharpness.

The depletion regions of infrared diode arrays are separated by the conducting HgCdTe bulk. Therefore, capacitive coupling can only occur between the In bumps in the space between the infrared array and the Si multiplexer or in the multiplexer itself. Smaller In bumps and a filling epoxy, between the multiplexer and the detector array, having a low dielectric constant help to minimize the coupling.

The Si-PIN diode array which we investigated is hybridized to the same Hawaii-2RG multiplexer as the HgCdTe infrared array, but has a much larger interpixel coupling capacitance. Hence, the main contribution to the interpixel capacitance must be located in the fully depleted Si-PIN diode array itself. It will be a challenge to substantially reduce this coupling.

References

[1] G. Finger, R. Dorn, M. Meyer, L.Mehrgan, J. Stegmeier, A. Moorwood, Nucl. Instr. and Meth. A 549, p 79-86, 2005.
[2] D. F. Figer, M. Regan, E. Morse, Independent Testing of Silicon PIN Detector Arrays for LSST, AAS 205th Meeting, Session 108 LSST, 2005.
[3] D. J. Schröder, Astronomical Optics, 2nd ed, Academic Press, San Diego, CA, 2000, Ch 17.1.c.
[4] N. Bezawada, D. Ives, Scientific Detectors for Astronomy 2005, Springer, Dordrecht, p. 499, 2005.
[5] G. Dalton, M. Cladwell, K. Ward, M. Whalley, K. Burke, J. Lucas, T.Richards, M. Ferlet, R. Edeson, D. Tye, M. Strachan E. Attad-Etegui, M. Leclerc, A. Galie, N. Bezawada, P. Clark,N Bisoauth, P. Luke, N. Dipper, P. Berry, W. Sutherland, J. Emerson, Proc. SPIE vol. 5489, p 46, 2004.
[6] G. Woodhouse. Privete communication, 2005
[7] D. Hall, G. Luppino, K. Hodapp, J. Garnett, M. Loose, M. Zandian, Proc. SPIE 5499, p 1-13, 2004.
[8] S. Gillessen et al., The Messenger 120, p. 26-32, 2005.
[9] J. Pirard, M. Kissler-Patig, A. Moorwood, P. Biereichel, B. Delabre, R. Dorn, G. Finger et al, Proc SPIE 5492, p. 1763, 2004.
[10] R. Sharples, R. Bender, M. Lehnert, K. Ramsay Howat et al., Proc SPIE 5492, p. 1179, 2004.
[11] S. D'Odorico, M. Andersen, P. Conconi, V. De Caprio et. al. Proc SPIE 5492, p. 220, 2004.
[12] M. Loose, J. W. Beletic, J. Blackwell, D. Hall S. Jacobson, Scientific Detectors for Astronomy 2005, Springer, Dordrecht, p. 699, 2005.
[13] G. Finger, R. Dorn, M. Meyer, Manfred, L. Mehrgan, J. Stegmeier, A. Moorwood, Proc. SPIE 5499, p 47, 2004.
[14] M. Loose, J. Beletic, J. Blackwell, J. Garnett, S. Wong, D. Hall, Proc SPIE 5492, p. 1395, 2004.
[15] G. Finger, J. Beletic, R. Dorn, M. Meyer, L. Mehrgan, A.F.M. Moorwood, J. Stegmeier, Scientific Detectors for Astronomy 2005, Springer, Dordrecht, p. 477, 2005.
[16] J. R. Janesik, Scientific Charge-Coupled Devices, SPIE Press, p. 134, 2001.
[17] A. Moore, Z. Ninkov, W. Forrest, Proc. SPIE 5167, p. 204-215, 2003.
[18] J. Garnett, private communication, 2005.